Comparing soil erodibility predictions against the fundamental understanding of erosion

M. van Damme[1], and J. Riteco[2]

[1] *Delft University of Technology, Delft, 2600 GA, The Netherlands*

[2] *ETH Zurich, 8006, Zurich, Switzerland*

Abstract

In breaching of levees, sediment erosion is induced by high flow velocities. Due to the often continuously accelerating flow, no equilibrium transport conditions are reached. The erosion rate is often described by the erosion equation which linearly relates the erosion rate to the excess shear stress by means of a soil erodibility coefficient. The soil erodibility is thereby often determined by means of the JET test. In the field of Dredging Engineering the study of the behaviour of sand under high flow velocities has also been an area of interest. At Delft University, the department of Dredging Engineering has performed several experiments on the behaviour of non-cohesive material when subjected to high flow velocities. It was noted that the initial porosity, and permeability of the material are important parameters to account for in the erosion process. This corresponds with observations that soil erodibility is sensitive to variations in material texture, compaction moisture content and compaction energy. It was furthermore noted that soil no longer erodes due to the pick-up of individual particles but fails as entire layers when subjected to high flow velocities. For shear failure to occur in non-cohesive soils the soil needs to dilate. The associated increase in pore volume causes an inflow of water into the soil. Based on the fundamental mass and momentum balance equations that describe the process of dilation of a bed when subjected to shear, a new process based erosion equation has been derived, which when validated against erosion measurements from the dredging industry shows promising results. This paper compares the prediction of soil erodibility by means of a JET test to the outcomes of the process based erosion equation. The paper highlights important differences and attempts are made to explain these.

1 Introduction

Overtopping can cause levees to fail whereby the overflowing water starts to erode the soil and initiate a breach. To assess the consequences of such an event it is important to assess how rapidly such a breach forms and expands. The rate of breach formation is often related to the soil erodibility which is considered to be a function of soil properties. In the case of overflowing levees soil properties change with time as the soil saturates. This could indicate that the soil erodibility is a dynamic process (Wang et al., 2014). Ezeabasili et al. (2014) noted that soil erodibility depends on various soil properties such as textures, soil aggregation, shear strength, infiltration capacity, permeability, organic content, chemical content, soil profile, surface stoniness, detaching/transportation force. Morris et al. (2008) identified material texture, compaction moisture content and compaction energy to most significantly affect soil erodibility based on research over the last decade by Hanson et al. (2001), Hanson and Cook (2004), Hanson et al. (2005a, 2005b, 2005c), Hunt et al. (2005) and Hanson and Hunt (2007). Hanson and Hunt (2007) observed that soil erodibility can clearly vary by several orders of magnitude as compaction water content and compaction effort are varied. Soil on a slope is also significantly more sensitive to erosion than soil on a flat surface as indicated by the retreat of the landside slope towards the water side slope during the early stages of breach formation (Visser, 1998). Although the importance of the factors affecting soil erodibility have been identified, no mention is made as to how to integrate these parameters into an erosion model (Morris et al. 2008).

The rate of erosion is often predicted by the erosion equation which states that the erosion rate is the product of the soil erodibility and the excess shear stress which is defined as the applied shear stress minus the critical shear stress. For shear stresses, which far exceed the critical shear stress, the significantly higher rates of erosion on the slope than on a flat surface cannot be explained from the increase in applied shear stresses on the slope. Consequently additional factors are applied in the erosion equation to account for the reduced stability of particles on the slope. The soil erodibility in this equation is thereby difficult to predict.

During breach formation flow velocities are high. The empirical nature of the erosion equation thereby requires ample data to be available for validation. Performing erosion experiments whereby soil is subjected to high flow velocities is however challenging due to the volatile behaviour of the erosion process, leading to a data shortage. This highlights the need for methods to quantify erosion rates which are based on a profound understanding of how soil surfaces respond when subjected to high shear stresses.

In this paper a process based erosion relationship is given which explains the effects of the moisture content, compaction energy, and slopes on the erosion rates. Section 2 describes the method along which the new relationship was derived, and Section 3 describes the experiments that have been performed to identify the soil erodibility.

2 A process based erosion relationship

Current erosion relationships relate the erosion rate to the force balance of a particle via the Shields parameter (Van Rhee, 2010). A water flow over a soil induces drag, shear, and lift-forces on soil particles at the surface which are then transferred to the particles beneath. High flow velocities over a bed give high bed shear stresses which are then transferred to the lower lying layers. Van Rhee (2010) and Bisschop et al. (2016) identified that under the high shear stress conditions, that correspond with overflow velocities in excess of approximately 1.5 m/s, the process of erosion can be described by thin layers of soil being sheared off. The shear resistance of soil increases with depth due to an increase in contact pressures between particles. The shear resistance of soil follows from Coulombs law and is given by (Verruijt, 2001).

$$\tau_c = c + \sigma' \tan\phi \qquad 1$$

Here τ_c [N/m^2] is the critical shear stress or shear resistance, defined as the shear stress above which soil fails due to shear, c [N/m^2] is the cohesion, σ' [N/m^2] is the effective stress in the soil, and ϕ is the internal friction angle of soil. The effective stress σ' [N/m^2] in Equation 1 consists of the soil pressures σ [N/m^2] minus the pore water pressure W [N/m^2]. Takahashi (2009) noted that shear failures occur over the depth over which the shear stresses exceed the critical shear stress, denoted hereonwards by the shear depth *d* [m] (See Figure 1).

When dilatant soils are subjected to shear, the pore spaces in the soil increase over the shear depth. This increase in pore volume is accommodated by an inflow of water into the soil through the soil surface. A pressure gradient is required for water to flow. At the soil surface, water pressures are given by the hydrodynamic boundary pressures. A pressure gradient consequently only forms when the pore water pressures in the top layer of the soil decrease. This gives a rise in effective stresses σ' [N/m^2] and an increase in shear resistance (See Equation 1).

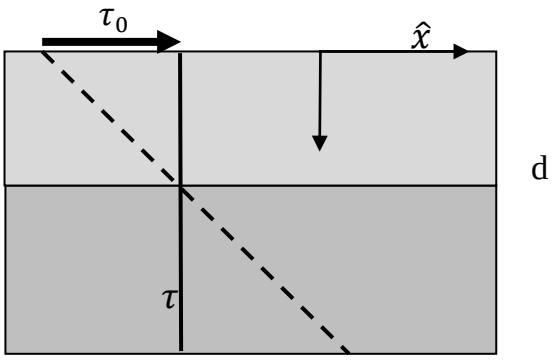

Figure 1. Stress strength relationship in non-dilatant soil.

The shear depth d [m] at which the shear stresses equal the critical shear stress consequently decreases (See Figure 2).

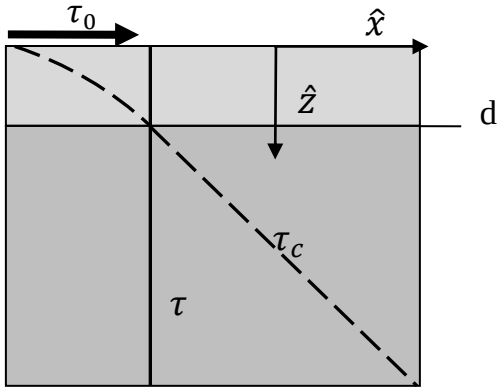

Figure 2. Stress strength relationship in dilatant soil.

Highly densified soils have a small initial pore space and consequently require a high degree of dilation in order to fail due to shear. Highly densified soils are also less permeable (Bisschop, 2016). The combination of the high inflow rates required for dilation and the low permeability, leads to low pore water pressures in the soil. The shear depth d [m] is therefore smaller than in the case of less densified soils. When erosion can be described by the continuous shear failure of thin layers of soil (Van Rhee, 2010, Takahashi, 2009), then dilatancy must influence the erosion process. The initial moisture content of the soil and the material texture respectively influence the shear depth by influencing the inflow rate and degree of dilatancy required for shear failures to occur. This corresponds with the observation that soil erodibility depends on material texture, moisture content, and compaction energy (Morris, 2008, Hanson and Hunt, 2007) Van Rhee (2010) noted that in the case where the ratio between erosion velocity and hydraulic conductivity exceeds a factor 3, the influence of permeability cannot be neglected any more. Although the impact of dilation has been identified, quantifying what the effects of dilation are on erosion, has been challenging. Winterwerp et al. (1992), Van Rhee (2010), and Mastbergen & Van den Berg (2003)

published sediment transport formulas for flow velocities up to several meters per second by trying to account for the drag experienced by the particles on the soil surface during inflow of water in the soil. These models give better predictions for the pick-up flux than the original sediment transport equations but still have a predominantly empirical nature (Bisschop et al., 2016). To overcome the drawbacks associated with the empirical nature of high speed erosion relationships the general description of the effects of dilatancy on the shear failure process has been extended into a process based erosion relationship.

The flow induced shear forces acting on the soil cause for the soil to be accelerated in the direction of the flow. Momentum is thereby transferred between the flow and the soil. To quantify the effects of infiltration and acceleration these processes have been described by the mass and momentum balance equations for the situation of an infinitely large soil surface which is subjected to an external shear stress. The soil surface is thereby denoted by the $\hat{\hat{x}} - \hat{y}$ plane. The positive $\hat{z}$-coordinate direction has been defined normal to the surface pointing into the soil. The $\hat{\hat{x}}$-coordinate direction is assumed to coincide with the direction of the shear stress which is applied to the surface (See Figure 2). The process of erosion has been accounted for by rewriting the resulting mass and momentum balance equations in terms of a moving coordinate system. The origin of the coordinate axes thereby moves along the $\hat{z}$--axis at a rate v [m/s] equal to the rate of displacement of the soil surface due to erosion. The resulting equations have then been integrated over the failure depth d [m] to relate the rate of erosion v [m/s] to the depth over which the shear stresses exceed the shear strength.

The volume balance equations now state that the rate of erosion v [m/s] is related to the relative velocity of the particles in the soil w_p [m/s] with respect to the pore water w_w [m/s] during dilation or,

$$-v\frac{(n_{loose}-n_0)}{1-n_{loose}} = n_{loose}\left(w_w - w_p\right)|_0 \qquad 2$$

The right hand side of Equation 2 thereby equals the specific discharge at the soil surface (Verruijt, 2006). The fraction on the left hand side of Equation 2 indicates the degree of dilation that is required for the soil layers to shear over each other. Here n_{loose} is the critical porosity at which the shearing of soil layers is possible, and n_0 is the in situ porosity of the dilatant material. The shear resistance is largely determined by the pore pressures which follow from the momentum balance equation for the pore water in the direction perpendicular to the soil surface. Subtracting the pore pressures from the soil pressures gives the effective stresses. Substituting these in Equation 1 gives the following expression for the critical shear stress $\tau_c|_d$ [N/m^2] at the shear depth d [m], as a function of the shear depth, and erosion velocity v [m/s].

$$\tau_c|_d = c + \tan\phi\,[(\gamma_s - \gamma_w)\cos(\alpha)\,d + (v + v_{min})\,\frac{\gamma_w d}{2K_s}\,\frac{(n_{loose}-n_0)}{1-n_{loose}}\Big] \qquad 3$$

Where v_{min} is the minimum inflow required to balance gravity induced shear stresses in the case of $0 < \alpha < \phi$. This minimum inflow velocity follows from

$$v_{min} = \left|\frac{2\gamma_s K_s}{\gamma_w}\,\frac{1-n_{loose}}{n_{loose}-n_0}\sin\alpha\right| \qquad 4$$

Equation 3 shows that the critical shear stress $\tau_c|_d$ [N/m^2] is governed by the effects of gravity and the effects of friction experienced during dilation. α is here the angle that the bed slope makes with the horizontal. Hence, for an increase in bed slope the contribution of the weight of the particles to the shear resistance decreases. Furthermore, γ_s [N/m^3] is the specific weight of soil, γ_w [N/m^3] is the specific weight of water, and K_s [m/s] is the saturated hydraulic conductivity. The shear stress at the shear depth $\tau|_d$ [N/m^2] has been expressed in terms of the erosion rate v [m/s] and the bed shear stress $\tau|_0$ [N/m^2] by integrating the horizontal momentum balance equation over the shear depth, leading to

$$\tau|_d = \tau|_0 - (v + v_{min})[(1-n_0)\rho_p u_p|_0 + n_0\rho_w u_w|_0] \qquad 5$$

where the effects of slope gradients on the shear stress, shear strength and momentum exchange have been accounted for via the use of v_{min} [m/s] in Equations 3 and 5. In the case of an unstable bed due to high surface shear stresses, a slope therefore contributes to erosion due to additional inflow required to counteract the shear forces due to gravity.
Here ρ_p [kg/m^3] is the particle density, and ρ_w[kg/m^3] is the density of water. Similarly u_p [m/s] and u_w [m/s] are respectively the velocity component of the particles and water in the direction of the main flow at the bed. These have been estimated by the shear velocity, whereby $u_p = u_w = \sqrt{\tau/\rho_w}$. $f_1 = 1$ indicates the absence of a groundwater flow parallel to the sloping bed; $f_1 = 0$ indicates the presence of a groundwater flow parallel to the bed slope. The last two terms in Equation 5 account for the momentum required to accelerate the particles and pore water. Equations 3 and 5 show that both the shear stress $\tau|_d$ [N/m^2], and shear resistance $\tau_c|_d$ [N/m^2] depend on the erosion rate v [m/s] and shear depth d [m]. A theoretical horizontal stress balance is obtained between the active and resisting forces for different combinations of the erosion rate v [m/s] and the shear depth d [m]. In order to arrive at an erosion relationship an extra expression is required to determine the most likely combination of the shear depth and erosion rate.

During erosion the surface shear stresses are transferred to the soil layers below causing the soil to dilate. The transfer of the horizontal stresses between the soil particles in the bed is optimum for a situation for which

the average effective stresses in the bed are maximum. This corresponds with a situation for which the shear depth averaged shear resistance is maximum. An expression for the averaged shear resistance follows from assuming that the degree of dilation over the shear depth is constant. The flow rate consequently decreases linearly over d, is maximum at the soil surface, and 0 at the shear depth d [m]. The contributions of the pore water pressures and soil weight to the shear depth averaged shear resistance are given by Equation 5.

$$\bar{\tau_c} = c + \tan\phi\, d\, \left[\frac{1}{2}(\gamma_s - \gamma_w)\cos(\alpha) + \frac{1}{2}\gamma_s \sin(\alpha) + \frac{\gamma_w v}{3K_s}\frac{(n_{loose} - n_0)}{1 - n_{loose}}\right] \quad 6$$

The shear depth d [m] in Equation 6 has been determined from Equations 3 and 5 by setting $\tau'|_d = \tau_c|_d$. The variations in average shear resistance $\bar{\tau_c}$ [N/m^2] as a function of the rate of displacement of the soil surface due to erosion v [m/s] have been displayed in Figure 3 which clearly shows that a unique combination of d [m] and v [m/s] gives a maximum in average shear resistance.

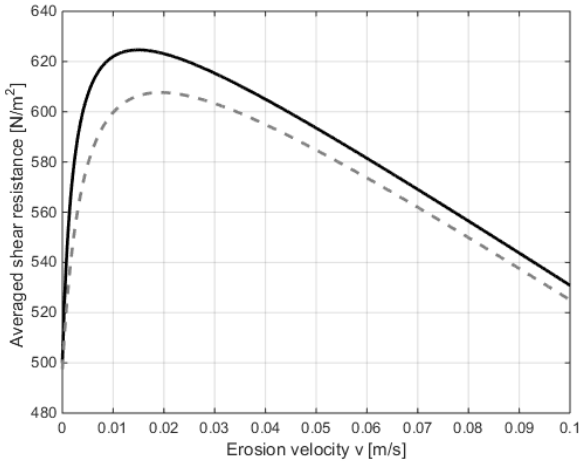

Figure 3. Average shear resistance as a function of the erosion rate. The values are given for $\tau_0 = 100\mathrm{N/m^2}$, $K_s = 2.5E-4$ m/s, $n_{loose} = 0.5$ and $n_0 = 0.4$. The maximum indicates the point where the average shear resistance is optimum.

3 Evaluation of the process based erosion relationship

The hypothesis that the erosion rate is given by the rate of displacement for which the average shear resistance is maximum has been evaluated using the experimental data provided by Bisschop et al. (2016), by evaluating the sensitivity of the input parameters based on generic observations, and by evaluating the results against the outcome of JET erosion tests.

3.1 Comparison against erosion tests under high flow velocities

Bisschop et al. (2016) performed erosion tests under high flow velocities on a horizontal bed ($\alpha = 0; v_{min} = 0$) of Geba sand with a d_{10} of 92 µm, a d_{50} of 125 µm, and a d_{90} of 145 µm. The permeability of the Geba sand was determined for various porosities. For a porosity $n = 0.4$ the permeability was approximately 5E-5 m/s (Bisschop et al. 2016). The hydraulic conductivity was found to increase logarithmically for an increase in porosity leading to a hydraulic conductivity of respectively 1E-4 m/s for $n = 0.45$ and 5E-4 m/s for $n = 0.5$. The maximum and simultaneously critical porosity was found to be 0.506, whereas the minimum porosity was 0.37. The initial density of the sand was between 1850 kg/m^3 and 1900 kg/m^3. Errors in the prediction of the shear stress varied between 10 and 80%. The prediction of the erosion rates were expected to vary between 20 and 40% (Bisschop et al. 2016).
For those tests for which Bisschop et al. (2016) provided the bed shear stress v[m/s] those erosion rates v [m/s] were determined the average shear resistance is maximum. The predicted erosion rates were converted into a pick-up flux by multiplying them with the density of the bed which was 1900 kg/m^3. Figure 5 shows the comparison between the predicted and measured pick-up flux (Bisschop et al. 2016).

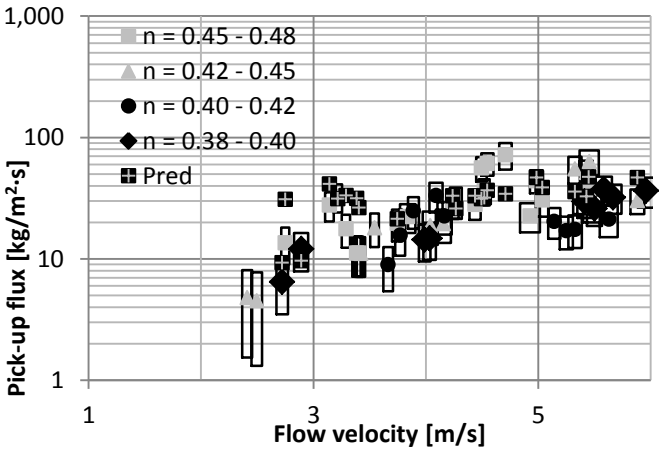

Figure 4. Measured versus predicted (Pred) values for the erosion rate under high flow velocities. The boxes indicate the error bars, after Bisschop et al. (2016).

The predictions show the same trend as the measurements. The corresponding proportionality between the shear stress and erosion rates thereby falls within the range of values for dilatancy reduced pickup functions identified by Bisschop et al.(2016).

3.2 Evaluating the sensitivity of the input parameters

To further evaluate the hypothesis that the erosion rate is given by the rate of displacement for which the average shear resistance is maximum, the impact of the slope and hydraulic conductivity on the erosion rate

have been evaluated, whereby n_0 = 0.4, and n_{loose} = 0.5. Figure 5 shows that the erosion rate significantly increases for an increase in bed slope angle and/or hydraulic conductivity. The water level is thereby assumed to follow the bed slope. Unlike the empirical erosion equation, the method provided here gives significantly higher predictions for the erosion rate on a slope than on a flat surface. This is in line with the observations that under equal shear stress conditions the erosion rates on a slope are significantly higher than on a flat surface (Visser, 1998).

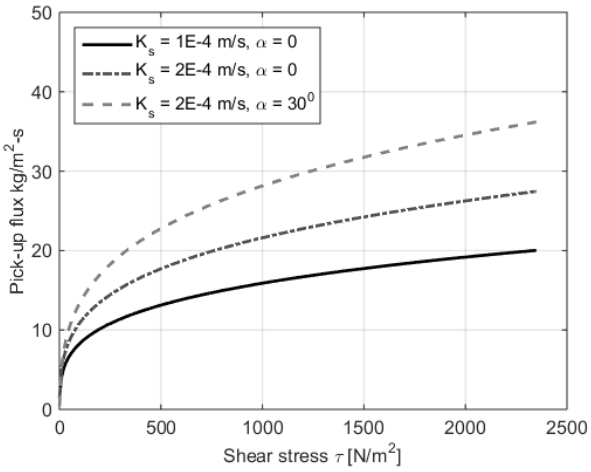

Figure 5. Erosion rates as a function of the bed shear stress for several values for the hydraulic conductivity and bed gradient.

Both the hydraulic conductivity and the degree of dilatancy required for shear failures to occur, depend on the porosity. Consequently the erosion rate predictions are sensitive to the values for the initial porosity compared to the critical porosity of the material, which agrees with observations made by Van Rhee (2010) and Bisschop et al. (2016). The porosity and hydraulic conductivity of soil are influenced by the compaction energy and compaction moisture content, which Morris et al. (2001) identified to be important factors that influence soil erodibility. In the new theory presented herein the effects of the moisture content and compaction energy are hence explained and accounted for via the hydraulic conductivity and porosity. Consequently, the relationship between the erosion rate and the excess shear stress is assumed to be non-linear whereby the power coefficient is smaller than 1. This conflicts the observations made during Jet Erosion Tests which are therefore discussed below.

3.3 Comparison against Jet Erosion Tests.

Riteco (2017) performed jet erosion tests with a submerged jet to determine the soil erodibility of sand (Sang et al., 2015). The experimental setup consisted of a large tank made of acrylic glass to allow for visual observations. The construction is based on the information given by Hanson and Cook (2004) and the ASTM standard D5852 (2003). The tank has two equally spaced compartments. The first compartment was used as experiment tank and the second compartment as collection tank. From the experiment tank water can overtop into the collection tank through which a constant water level was maintained (See Figure 6). Connected to the tank is a water inlet, a water outlet from the collecting tank and a water outlet from the experiment tank which was used to regulate the water pressure at the bottom of the sand layer. This allowed for the effects of infiltration on soil erodibility to be evaluated. On top of the tank the JET equipment was installed to measure the erodibility of the sand.

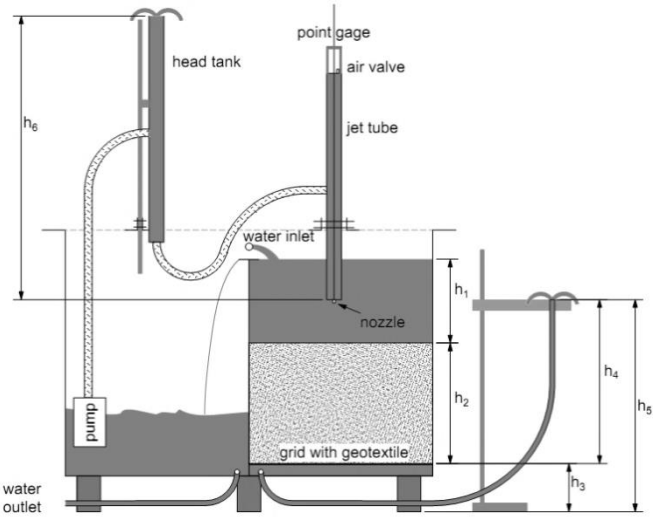

Figure 6. Schematic overview of the test tank used for the Jet Erosion Tests after Riteco (2017).

A schematic of the complete set-up is shown in Figure 6. Sand with grain diameters between 0.2 mm and 0.8 mm was chosen. The porosity of the sand was 41.8%. The erosion tests were conducted with jet head settings of respectively 795 mm and 450 mm resulting in different bed shear stresses. The development of the scour hole over time was monitored with a video camera. Since the equilibrium scour depth is reached rather quick each test had a duration of only around 45 seconds. Each experiment was repeated three times to identify outliers. The effects of infiltration on the erosion rate were found to be negligible for high stress conditions induced during the higher jet head and just after initiating the jet on the undisturbed sand bed.

The erodibility of the sand was determined with both the Blaisdell solution of Hanson and Cook (2004) and the scour depth method by Daly et al. (2013) under the assumption of a linear relationship between the excess shear stress and the erosion rate. The results are given in Tables 1 and 2.

Table 1. Results measurements for a head of 795mm

	Blaisdell method		Scour depth method	
	Mean	Std.	Mean	Std.
K_d [m^3/Ns]	0.0033	0.0006	0.0158	0.0029
τ_c [N/m^2]	0.7181	0.1535	2.3586	0.0727

During the experiments the hydraulic head was varied but the sand properties were kept the same and the height of the nozzle over the undisturbed sand bed was kept at 112 mm. Since the erodibility and critical shear stress are soil parameters, the results in Table 1 and Table 2 should be identical. However, especially in the case of the scour depth method the difference in prediction is significant.

Table 2. Results measurements for a head of 450mm

	Blaisdell method		Scour depth method	
	Mean	Std.	Mean	Std.
K_d [m^3/Ns]	0.0041	0.0009	0.0203	0.0045
τ_c [N/m^2]	0.5933	0.1150	1.6917	0.1522

The process based erosion equation presented in Section 2 indicates a relationship between the shear stress and the erosion rate given by $= K_d \tau^b$, where *b<1* (See Figure 5). Here K_d denotes a soil erodibility parameter. This non-linear relationship was evaluated by relating the erosion rates, measured immediately after initiating the jet on the undisturbed horizontal sand bed, to the shear stresses applied by assuming that K_d and *b* are constants. Working out this relationship gives

$$\frac{E_{795}}{\tau_{795}^b} = \frac{E_{450}}{\tau_{450}^b} \qquad 6$$

Where *E* refers to the measured erosion rate, and τ refers to the bed shear stress. The subscripts refer to the jet head in mm. For $\tau_{795} = 6.84$ N/m^2 and $\tau_{450} = 3.93$ N/m^2 , $E_{795} = 45.6$ mm/s and $E_{450} = 34.0$ mm/s, Equation 6 gives $b \approx 0.5$. This value for b corresponds well with the process based erosion relationship derived in Section 2. It should thereby be noted that any critical shear stress is not accounted for. Including a critical shear stress gives a further reduction in the power coefficient *b*. The resulting value of this power coefficient corresponds with the measurements performed by Bisschop et al. (2016), and the theoretical relationship described in Section 2.

As the scour hole develops, the flow follows the contours of the scour hole. As the scour hole deepens the curvature of the flow lines along the wall of the scour hole increases. A change in direction of the flow requires a reaction force from the soil on the flow. This reaction force induces a normal force on the bed. Further up the slope the soil profile is quite steep whereby the effects of gravity work in opposite direction of the main flow. Once a stable scour hole is developed the degree of dilation of the particles at the bed is 0 and the soil profiled must consequently be in a geotechnical equilibrium. Riteco (2017) performed a geotechnical stability analysis of the scour hole showing that it is geotechnically stable. For a parallel flow past a bed, the flow lines are straight indicating that the critical shear stress is lower than follows from the Jet Erosion Tests. Hence, the results of the Jet Erosion Test may be used to further evaluate the power relationship. Further tests with an ever higher jet power are thereby recommended.

4 Discussion

This paper shows that the erosion rate can be explained by means of the fundamental principles of soil mechanics by accounting for the effects of the momentum exchange and dilation. The erosion rate follows directly from the combination of shear depth and pick-up flux for which the average shear strength over the depth of failure is maximum. The erosion rate is thereby a function of the difference between the initial porosity and the critical porosity, the hydraulic conductivity, and the slope gradient. The predicted erosion rates agree well with experimental data (See Figure 4). The influence of the slope gradient, is thereby substantial (See Figure 5). This is in line with the observations that under equal shear stress conditions the erosion rates of material on a slope are significantly higher than for material on a flat surface (Visser, 1998). The material type, compaction efforts, and compaction moisture content all influence the initial and critical porosity of the dilatant bed material, and the hydraulic conductivity of the material. The effect of these parameters is thereby thus fundamentally explained and accounted for leading to more accurate erosion predictions. Validation of the erosion predictions against measurements on slopes is recommended.

5 Conclusions

This paper offers a process based erosion equation which provides a fundamental explanation of the effects of compaction and material type on erosion. Unlike any other erosion relationship used in the field of breaching this far, the method given here also explains the higher rates of erosion observed on a slope than on a flat surface. The method has been validated against experimental data. A need for a new method of evaluating the output of the Jet Erosion Test has thereby been highlighted as the current method does not explain the differences in soil erodibility observed when changing the jet head. Extension of this method to cohesive soils is recommended. In order to further refine the process based erosion equation described in this paper further experiments to the erosion rate under high flow velocities, and steep slopes are recommended.

References

ASTM. (2003). Standard Test Method for Erodibility Determination of Soil in the Field or in the Laboratory by the Jet Index Method. Annual Book of ASTM Standards, Vol. 04.08. American society for Testing and Materials.

Bisschop, F., Miedema, S., Visser, P., Keetels, G., and Van Rhee, C. (2016). "Experiments on the pickup flux of sand at high flow velocities." Journal of Hydraulic Engineering, 142(7).

Daly, E.R., Fox, G.A., Al-Madhhachi, A.T., Miller, R.B. (2013). A scour depth approach for deriving erodibility parameters from jet erosion tests. Transactions of the American Society of Agricultural and Biological Engineers, Vol. 56(6). pp. 1343-1351.

Ezeabasili, A.C.C., Okoro, B.U. & Emengini, E.J. (2014). Relative erodibilities of some soils from Anambra basin. Sky Journal of Soil Science and Environmental Management. Vol. 3(8). pp. 83-90.

Hanson, G.J. & Cook, K.R. (2004). Apparatus, test procedures and analytical methods to measure erodiblity in situ. Applied Engineering in Agriculture, Vol. 20(4). pp. 455-462.

Hanson, G.J., Cook, K.R. & Hunt, S.L. (2005a). Physiscal Modeling of Overtopping Erosion and Breach Formation of Cohesive Embankments. Transactions of the American Society of Agriculture Engineers, Vol. 48(5). pp. 1783-1794.

Hanson, G.J. & Hunt, S.L. (2007). Lessons learned using laboratory jet test method to measure soil erodibility of compacted soils. American Society of Agriculture and Biological Engineers, Applied Engineering in Agriculture. Vol. 23(3). pp. 305-312.

Hanson, G.J., Morris, M., Vaskinn, K., Temple, D.M., Hassan, M. & Hunt, S. (2005b). Research activities on the erosion mechanics of overtopped embankment dams. Journal of Dam Safety. Vol. 3(1). pp. 4-15.

Hanson, G.J., Robinson, K.M. & Cook, K.R. (2001). Prediction of headcut migration using a deterministic approach. Transactions of the American Society of Agriculture Engineers, Vol. 44(3). pp. 525-531.

Hanson, G.J., Temple, D.M., Morris, M., Hassan, M. & Cook, K. (2005c). Simplified breach analysis model for homogeneous embankments: Part II, Parameter inputs and variable scale model comparisons. Proceedings United States Society on Dams Annual Meeting and Conference, Salt Lake City, Utah. pp. 163-174.

Hunt, S.L., Hanson, G.J., Cook, K.R. & Kadavy, K.C. (2005). Breach widening observations from earthen embankment tests. Transactions of the American Society of Agriculture Engineers, Vol. 48(3). pp. 1115-1120.

Mastbergen, D. and Van den Berg, J. (2003). "Breaching in fine sands and the generation of sustained turbidity currents in submarine canyons." Sedimentology, 40(4), 625–637.

Morris, M., Hanson G. & Hassan, M. (2008). Improving the accuracy of breach modelling: why are we not progressing faster?. Journal of Flood Risk Management. Vol. 3(1). pp. 150-161.

Riteco, J. (2017) Effects of water infiltration on soil erodibility, MSc thesis ETH Zurich, Delft University of Technology, Delft, The Netherlands.

Sang, J., Allen, P. & Dunbar, J. (2015). Determination of critical shear stress of noncohesive soils using submerged jet test and turbulent kinetic energy. Earth Surface Processes and Landforms, Vol. 40(9). pp. 1182–1190.

Takahashi, T. (2009). "A review of Japanese debris flow research." International Journal of Erosion Control Engineering, 2(1).

Van Rhee, C. (2010). "Sediment entrainment at high flow velocities." Journal of Hydraulic Engineering, 136(9), 572–582.

Visser, J. P. (1998). "Breach growth in sand-dikes." Ph.D. thesis, Delft University of Technology, Delft, The Netherlands.

Verruijt (2001). Soil Mechanics. Delft University of Technology, <http://geo.verruijt.net/>.

Verruijt, A. (2006). Offshore Soil Mechanics. Delft University of Technology.

Wang, G., Wu, B., Zhang, L., Jiang, H. & Xu, Z. (2014). Role of soil erodibility in affecting available nitrogen and phosphorous losses under simulated rainfall. Journal of Hydrology Vol. 514. pp. 180-191.

Winterwerp, J., Bakker, J., Mastbergen, D., and Rossum, V. (1992). "Hyperconcentrated sand water mixture flows over erodible bed." Journal of Hydraulic Engineering, 118.